ORNL-4834

HEAVY-ION BEAM PROBE DESIGN CALCULATIONS FOR THE ORMAK AND ELMO BUMPY TORUS DEVICES

Gregory S. McNeilly

BLANK PAGE

Printed in the United States of America. Available from
National Technical Information Service
U.S. Department of Commerce
5285 Fort Royal Road, Springfield, Virginia 22151
Price: Printed Copy $3.00; Microfiche $0.95

ORNL-4834
UC-20 — Controlled Thermonuclear Processes

Contract No. W-7405-eng-26

MATHEMATICS DIVISION

HEAVY-ION BEAM PROBE DESIGN CALCULATIONS FOR THE ORMAK AND ELMO BUMPY TORUS DEVICES

Gregory S. McNeilly

NOTE

This work was done in cooperation with and supported by the Thermonuclear Division

FEBRUARY 1973

OAK RIDGE NATIONAL LABORATORY
Oak Ridge, Tennessee 37830
operated by
UNION CARBIDE CORPORATION
for the
U.S. ATOMIC ENERGY COMMISSION

TABLE OF CONTENTS

LIST OF FIGURES

HEAVY-ION BEAM PROBE DESIGN CALCULATIONS FOR THE ORMAK AND ELMO BUMPY TORUS DEVICES

Gregory S. McNeilly

ABSTRACT

Beam probes are a promising plasma diagnostic tool, since the heavy-ion beam is capable of sampling the plasma locally, thus allowing measurements of fine spatial resolution. It is desirable that the locus of points of second ionization of the beam - the detector line - be as nearly straight as possible and pass through the center of the plasma. This allows a more convenient unfolding of the experimental results. In addition, for ORMAK, intervening coils must be avoided as much as possible. These constraints, as well as the probe's physical limitations, determine the limits of the calculations described in this report. This work was sponsored by C. F. Barnett of the Thermonuclear Division.

I. INTRODUCTION

Figures 1 and 2 show the ORMAK and ELMO Bumpy Torus (EBT) devices. Extensive discussion of these devices and their use in controlled fusion research is described elsewhere.[1,2] The beam probe described here is similar to experimental apparatus in operation on the Princeton ST Tokamak[3] and will be described only briefly here.

Both ORMAK and EBT have their strongest vacuum magnetic fields directed toroidally. These toroidal or confining fields produce the predominate forces on the ions as they pass through the plasma region. Thus, to a good approximation, an ion in a vertical plane containing a major radius of the torus (in the case of EBT at the mid-plane of two coils) is deflected by the confining field only within that plane. Consequently, the calculation of the trajectory is reduced to two dimensions. The effect of in-plane or poloidal fields is discussed in detail below.

BLANK PAGE

Fig. 1. The ORMAK (Oak Ridge Tokamak) Device.

ORNL DWG. 71-13885

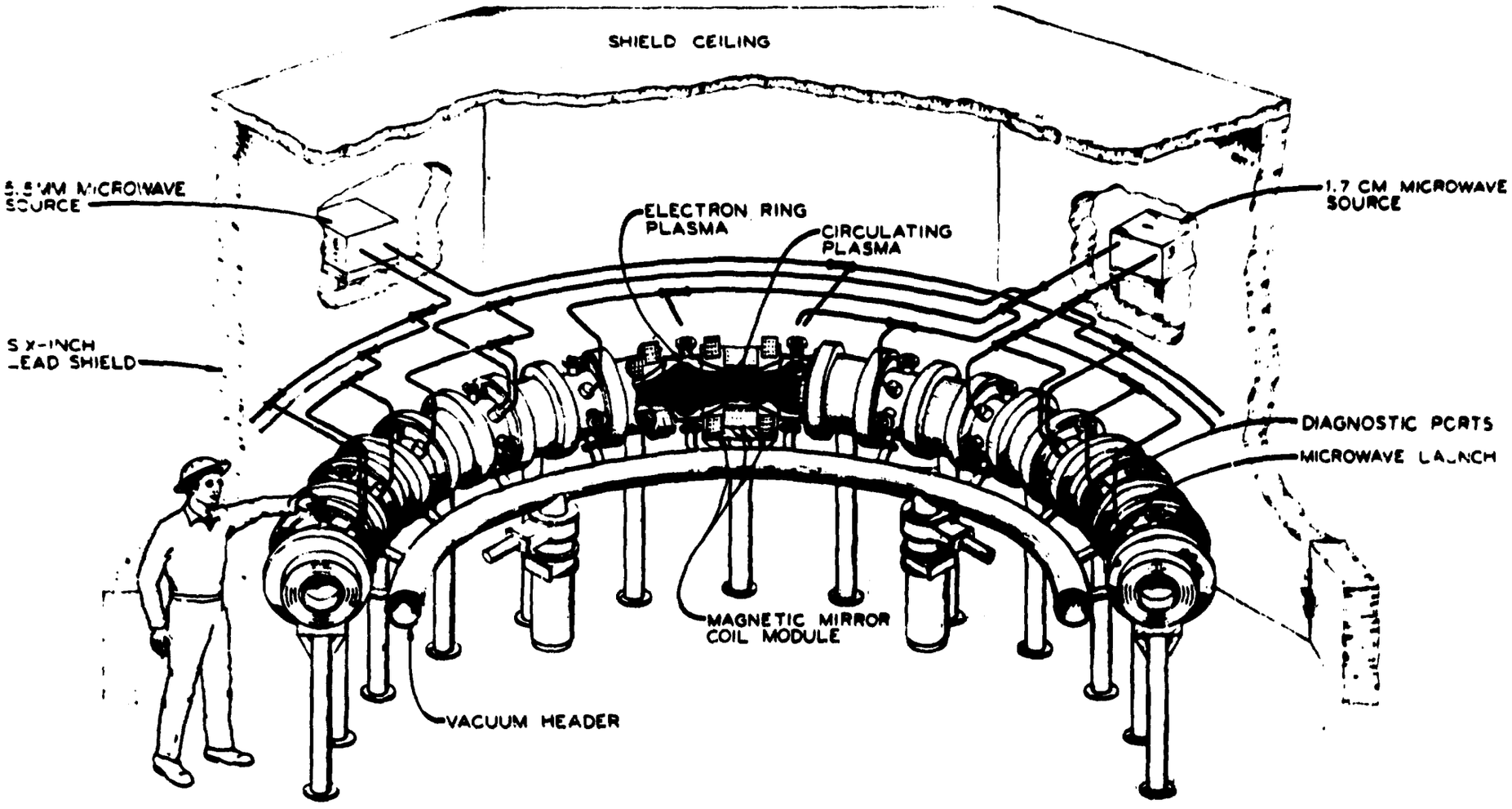

Fig. 2. The EBT (Elmo Bumpy Torus) Device.

As a singly charged beam of ions moves through the plasma, some ions collide with the electrons and become doubly ionized. At this point the singly and doubly charged beams diverge, since the Lorentz force differs by a factor of two. This separation begins at the point of ionization and thus provides a measurement of the plasma at a definite spatial position. It can be shown[3] that a comparison of the 1^+ and the 2^+ beams gives a measure of the electron density, space potential, and the component of the vector potential along the confining field lines at the point of second ionization. Consequently, sweeping the ion beam through the plasma volume as a function of time allows one to measure a locus of points. If the sweep time is much shorter than the plasma relaxation time, one then obtains a "snapshot" of the plasma volume at these points. When the grid of points, i.e. the detector line, is fairly straight and passes through the center of the plasma, one can measure radial distributions of the plasma parameters. In the figures of trajectories to follow, the diamonds indicate the grid of points of second ionization.

II. Trajectory Calculations

The following description applies to both ORMAK and EBT since only the B-field calculation is different for the two cases.

The motion of a charged particle in an electromagnetic field is governed by the Lorentz force

$$\vec{F} = q[\vec{E} + \vec{v} \times \vec{B}] \ , \qquad (2.1)$$

where q is the charge on the particle, $\vec{E}$ is the electric field, $\vec{v}$ is

the velocity of the particle, and $\vec{B}$ is the magnetic field. Expressing Eq. 2.1 in a more mathematical notation, one has

$$\frac{d^2}{dt^2}\vec{r}(t) = \frac{q}{m}\left[\vec{E}(\vec{r},t) + \frac{d}{dt}\vec{r}(t) \times \vec{B}(\vec{r},t)\right] . \qquad (2.2)$$

Equation 2.2 is a second order, ordinary differential equation, and thus may be expressed as a system of coupled first order ordinary differential equations using the substitution

$$\frac{d}{dt}\vec{r}(t) = \vec{v}(t) . \qquad (2.3)$$

Using Eq. 2.3 in Eq. 2.2, one obtains

$$\frac{d}{dt}\vec{v}(t) = \frac{q}{m}\left[\vec{E}(\vec{r},t) + \vec{v}(t) \times \vec{B}(\vec{r},t)\right] \qquad (2.4)$$

The simultaneous solution of Eq. 2.3 and Eq. 2.4 is completely equivalent to the solution of Eq. 2.2. In the present calculation, Eq. 2.4 is simplified by setting $\vec{E}(\vec{r},t) = 0$, and $\vec{B}(\vec{r},t) = \vec{B}(\vec{r})$, i.e. the magnetic field is constant in time. The numerical solution of simultaneous first order ordinary differential equations is straightforward, and in the present case a self-adjusting Runge-Kutta program is used.[4] The solution of Eq. 2.3 and Eq. 2.4 gives $\vec{r}(t)$, i.e. the trajectory of the charged particle. Given a set of initial conditions, the trajectory is uniquely determined.

The object of the calculation is to obtain a detector line - the locus of points of second ionization - which is fairly straight, not too oblique to the ion trajectories, and which passes through the center of the plasma. These requirements affect the choice of initial conditions.

Given the B field, input to the calculation is:

R_B - the radius of B field cut-off,

R_1 - the radius of the source point,

R_2 - the radius of the detector,

r_o - the radius of the limiter for ORMAK,

E - the ion energy,

M - the ion mass,

S_o - the point of entrance into the B field region of the central trajectory,

as well as numerous internal parameters requiring prescribed accuracy, initial step size, etc.[4] The angle at the point of entrance is varied until a trajectory passes through the center of the plasma. This angle, along with R_1 determines the position of the source. The charge of the ion is changed from 1^+ to 2^+ at the plasma center, and the trajectory is continued. The intersection of the ion path and the R_2 radius determines the position of the detector. With the source and detector fixed, a series of trajectories at different entrance angles is calculated to sweep through the plasma volume. The point of second ionization of each trajectory is determined as follows. The path of the 1^+ beam is calculated. If the path misses the detector due to an excessive deflection by the B field, the calculation of the path is abandoned. However, if the path misses due to insufficient deflection, a point of second ionization at the middle of the path is chosen and the trajectory recalculated from that point. The program then performs an iteration on the point of second ionization, moving the point to an earlier position on the path if more deflection is required, or to a later position on the path if less

deflection is required, until intersection with the detector is obtained. When this calculation has been repeated for all the trajectories at different entrance angles, the locus of points of second ionization represents the detector line - so called, because the signal in the detector originates only from this line in the plasma. For a given ion and a given entrance point S_o, one may vary R_1, R_2, and E to affect the shape of the detector line. The results of calculations for ORMAK and EBT are described in Section IV below.

III. Lens Calculations

The angular spread of rays from the source required to sweep across the plasma volume is wider than can be conveniently supplied by sweep plates. A parabolic lens can be used to magnify the angle produced by conventional sweep plates. This parabolic lens, as the name implies, has a parabolic variation in voltage, i.e.

$$V(y) = V_o(y/y_\ell)^2 \ , \tag{3.1}$$

where V_o is the maximum voltage, and y_ℓ is the half width of the lens (see Fig. 3). Since

$$\vec{E} = - \nabla V \ , \tag{3.2}$$

there is a non-zero value for only the y-component of the E field, and thus the motion of the ions through the lens is confined to the x-y plane. After the ion emerges from the sweep plates, it moves in a straight line in the force free Regions 1 and 3, so deflection occurs only in Region 2. The equation of motion in Region 2 is

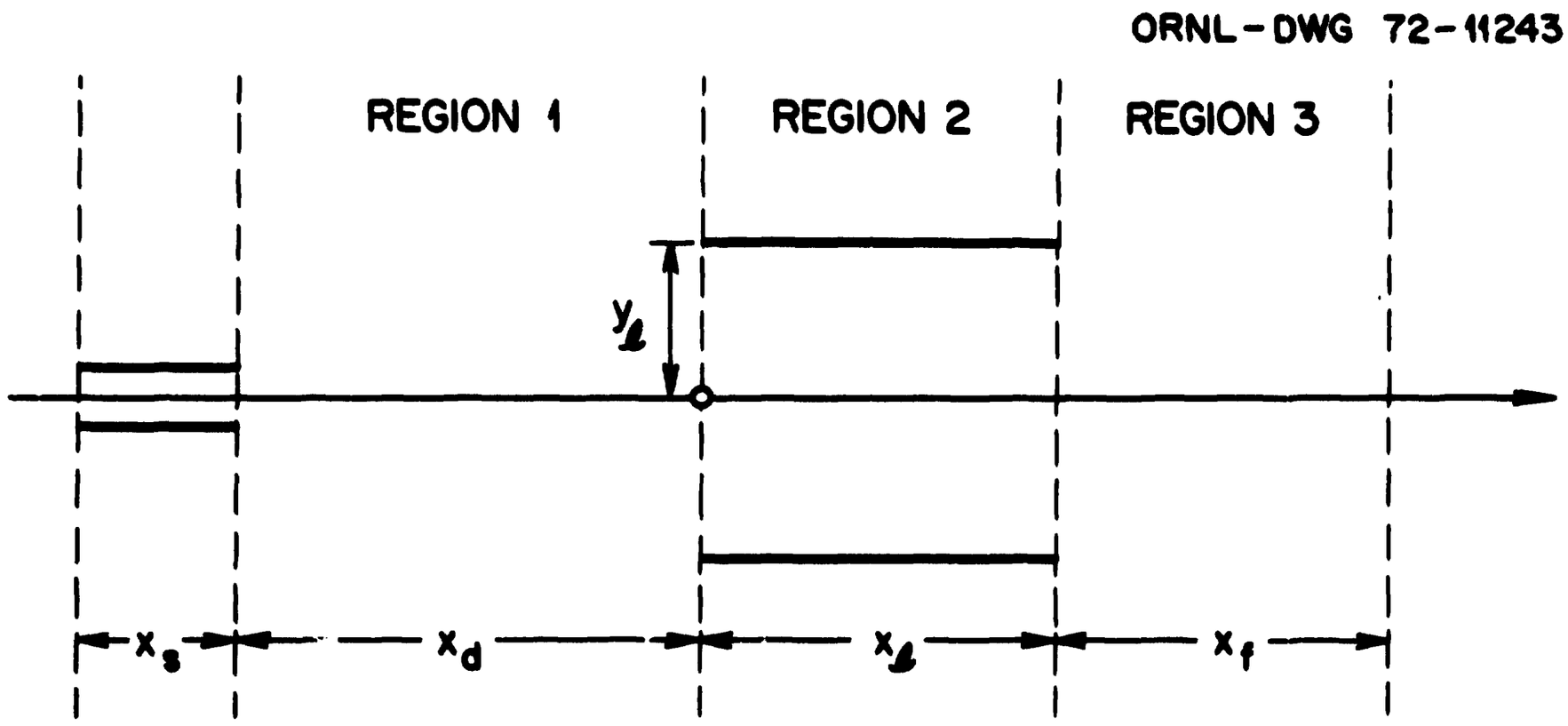

Fig. 3. Sweep Plates and Lens Geometry - Side View. The origin of co-ordinates used in Section III is indicated by the circle.

$$m \frac{d^2}{dt^2} y = q E_y \ , \tag{3.3}$$

where $E_y = - 2V_o y/y_\ell^2$. Equation 3.3 can be written as

$$\frac{d^2}{dt^2} y + cy = 0 \ , \tag{3.4}$$

where $c = 2V_o q/my_\ell^2$. The solution of Eq. 3.4 is

$$y = A \sin \sqrt{c}\, t + B \cos \sqrt{c}\, t \ , \tag{3.5}$$

where A and B are constants determined by the initial conditions. Since the velocity in the x direction is a constant determined by the ion energy, time may be eliminated from all equations by the relation $t = x/v_x$. With the equation of motion known in all three regions, the focal length and sweep angle of the lens can be calculated by matching the equations of motion at the region boundaries. If one chooses origin as shown in Fig. 3, the equations are

Region 1
$$y = y_2 + \frac{y_2 - y_1}{x_d} x \ , \tag{3.6}$$

Region 2
$$y = \frac{v_{y_2}}{\sqrt{c}} \sin \frac{\sqrt{c}\, x}{v_x} + y_2 \cos \frac{\sqrt{c}\, x}{v_x} \ , \tag{3.7}$$

Region 3
$$y = y_3 + v_{y_3} \frac{(x - x_\ell)}{v_x} \ , \tag{3.8}$$

where the numbered subscripts refer to positions and velocities at the left hand side of each region. The focal length of the lens (i.e. the length beyond the right hand side of the lens) is

$$x_f = - \frac{v_x y_3}{v_{y_3}} \ , \tag{3.9}$$

and the sweep angle α of the lens is

$$\frac{\alpha}{2} = - \tan^{-1} [v_{y_3}(\max)/v_x] \tag{3.10}$$

where the $v_{y_3}(\max)$ is for the outermost possible trajectory through the lens. Equation 3.9 and Eq. 3.10 are determined by y_3 and v_{y_3} which are given by

$$y_3 = \frac{v_{y_2}}{\sqrt{c}} \sin \sqrt{c}\, \frac{x_\ell}{v_x} + y_2 \cos \sqrt{c}\, \frac{x_\ell}{v_x} , \tag{3.11}$$

$$\text{and } v_{y_3} = v_{y_2} \cos \sqrt{c}\, \frac{x_\ell}{v_x} - y_2 \sqrt{c} \sin \sqrt{c}\, \frac{x_\ell}{v_x} , \tag{3.12}$$

where for the case of parallel sweep plates

$$v_{y_2} = \frac{y_2 v_x}{x_s/2 + x_d} . \tag{3.13}$$

Thus the focal length is independent of y_2, and the sweep angle is known as a function of y_2. To obtain $v_{y_3}(\max)$, one needs $y_2(\max)$ in Eq. 3.12 where

$$y_2(\max) = y_\ell \Big/ \left[\frac{v_x}{(x_s/2 + x_d)\sqrt{c}} \sin \sqrt{c}\, \frac{X_i}{v_x} + \cos \sqrt{c}\, \frac{X_i}{v_x} \right] \tag{3.14}$$

and the inflection point X_i is given by

$$X_i = \frac{v_x}{\sqrt{c}} \tan^{-1} [v_{y_2}/y_2 \sqrt{c}] . \tag{3.15}$$

Equation 3.9 - Eq. 3.15 provides a closed form solution for the focal length and sweep angle of the lens. The parameters x_s, x_d, x_ℓ, y_ℓ, V_o, and v_x can be varied to study their effects.

If a beam of radius y_o is considered, the lens introduces a transverse dispersion which can be significant for some parameter values. The above equations apply, with y_2 replaced by $y_2 \pm y_o$ in Eq. 3.13

for the bottom and top of the beam respectively (thus also affecting Eq. 3.15), y_ℓ replaced by $y_\ell - y_f$ in Eq. 3.14, where y_f is the displacement due to the finite beam - i.e. zero for the top of the beam, $2y_o$ for the bottom of the beam - and the first term in the bracket of Eq. 3.14 multiplied by $1 \pm y_o/y_2(\max)$. In this case Eq. 3.14 becomes transcendental, and $y_2(\max)$ must be iterated to obtain a solution. The results of the lens calculations are discussed in Section V below.

IV. Results of Trajectory Calculations

For ORMAK and EBT, the vacuum B fields in the vertical plane are calculated using an ORNL version of the MAFCO computer code.[5] Three dimensional ORMAK calculations, including the effect of the plasma current, used an analytic approximation for the total field which is described below. Only two dimensional calculations have been performed for EBT. An approximation to simulate the effect of the high-beta annulus in EBT[2] is described below.

The ORMAK vacuum B field is well approximated by

$$B_z(x) = \frac{B_o \cdot R_o}{(x+R_o)} , \tag{4.1}$$

where R_o is the major radius of the torus, B_o is the B field in the middle of the minor cross section of the torus, and x is measured from an origin located at the middle of the minor cross-section (see Fig. 4). At the inner radius of the confining field coils, the B field falls rapidly toward zero. The poloidal B field due to the plasma current is approximated by

$$B_\phi(r) = \frac{\mu_o I}{\pi r_c^2}\, r \left[1 - \frac{r^2}{2r_o^2}\right] \text{ for } r < r_o , \tag{4.2}$$

$$B_\phi(r) = \frac{I}{2\pi r} \text{ for } r > r_o , \tag{4.3}$$

ORNL-DWG 72-11244

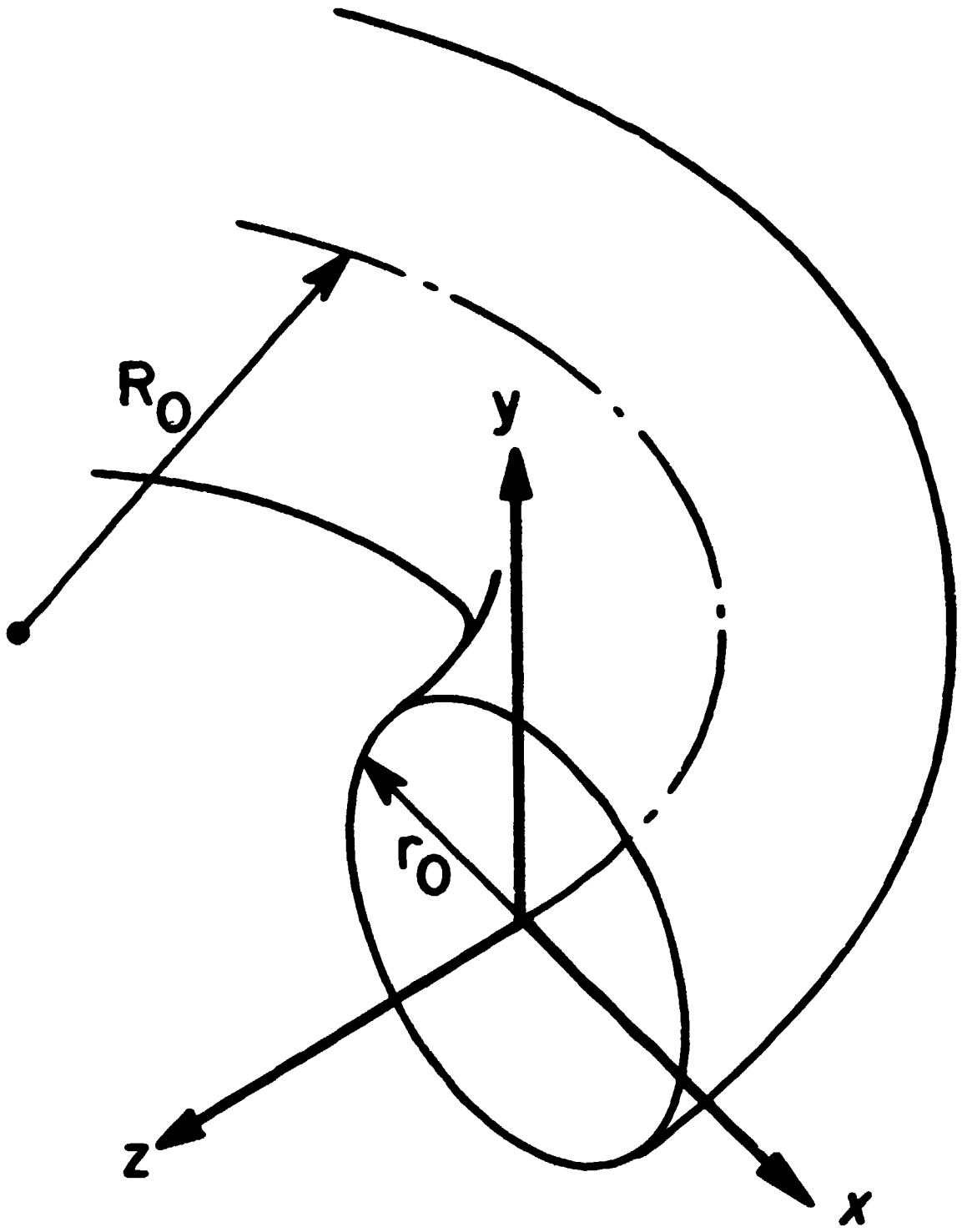

Fig. 4. The Co-ordinate System Used in the Equations of Section IV.

where r is a radius measured from the center of the minor cross section, μ_o is the vacuum magnetic permeability, I is the total plasma current flow (400,000 amperes), and r_o is the radius of the ORMAK limiter (23 cm). Equations 4.2 and 4.3 result from a parabolic plasma current fall-off ending at r_o, with a total current flow of I.

The effect of the poloidal field is to produce a z-displacement of the particle trajectories. The z-displacement depends on the geometry of detector and source as well as the beam energy. For a typical geometry (see Fig. 6), the z-displacement at the detector, due to the B field of Eqs. 4.1 to 4.3, is about 2 cm $\pm$ 1 cm. (Note that all trajectory figures list the ion energy in keV on the first line, then on the second line the source angle measured from the vertical axis, the detector angle measured from the source axis, and the source and detector radii in centimeters.) Since the z-displacement within the confining coils is less than the above, and since B_z is reasonably constant as a function of z, the calculation can be treated as a two-dimensional one, with the trajectories confined to a vertical plane of the torus. The figures of trajectory calculations shown are all two dimensional.

When the source and detector radii are sufficiently large, the detector line is straight and at approximately a 45° angle to the ion trajectories (see Fig. 5). A more transverse detector line improves resolution as can be seen by imagining a parallel ion trajectory and detector line. In this case the point of second ionization could be at any point on the trajectory. Unfortunately, the larger radii such as shown in Fig. 5 define ion paths which are primarily intercepted by ORMAK coils. Thus, other geometries are necessary in order to optimize the beam's transmission through the device.

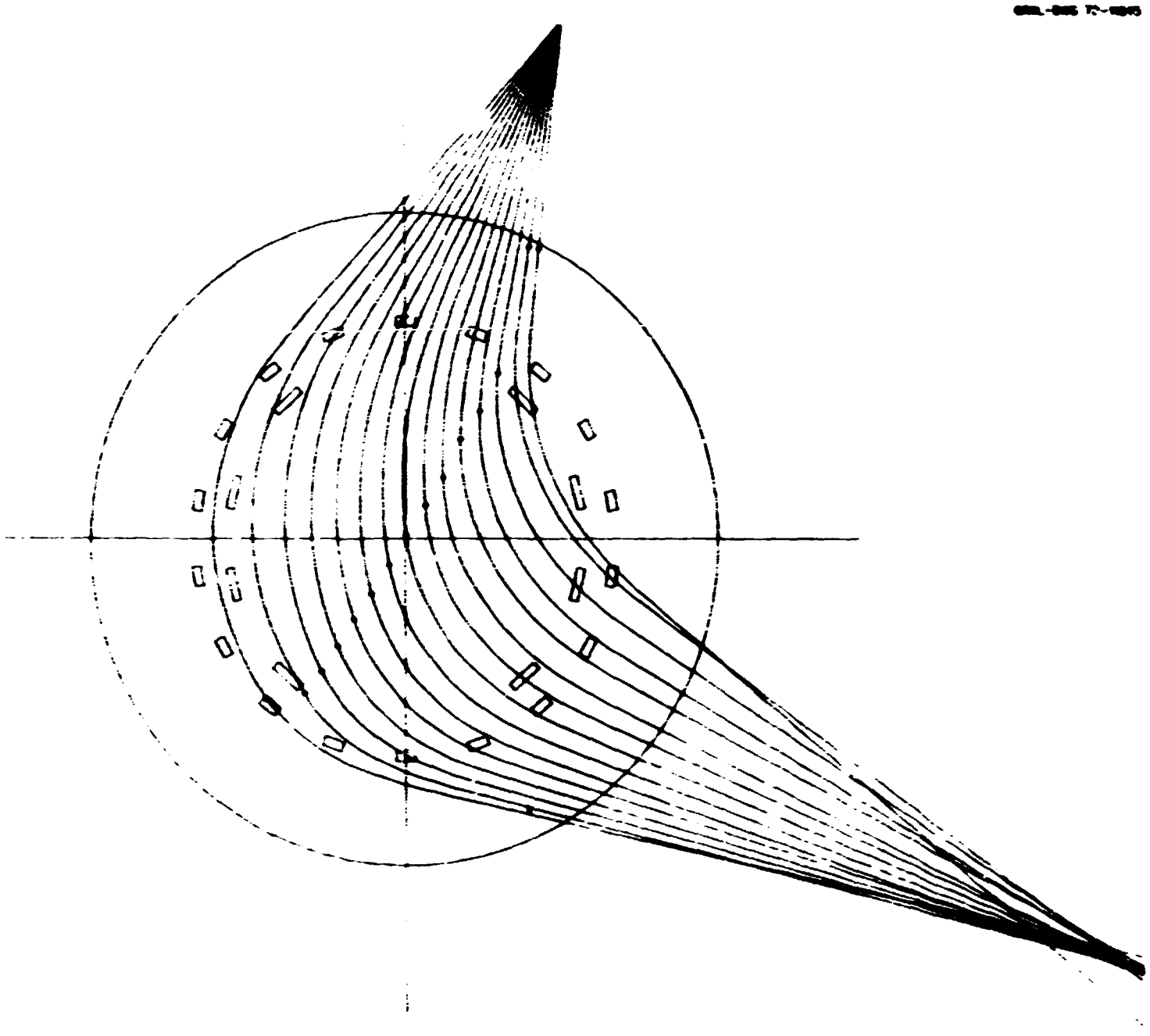

Fig. 5. "Straight Line" Geometry for ORMAK. Note that in all trajectory figures the ion energy is listed in keV on the first line, then on the second line the source angle measured from the vertical axis, the detector angle measured from the source axis, and the source and detector in radii centimeters are listed.

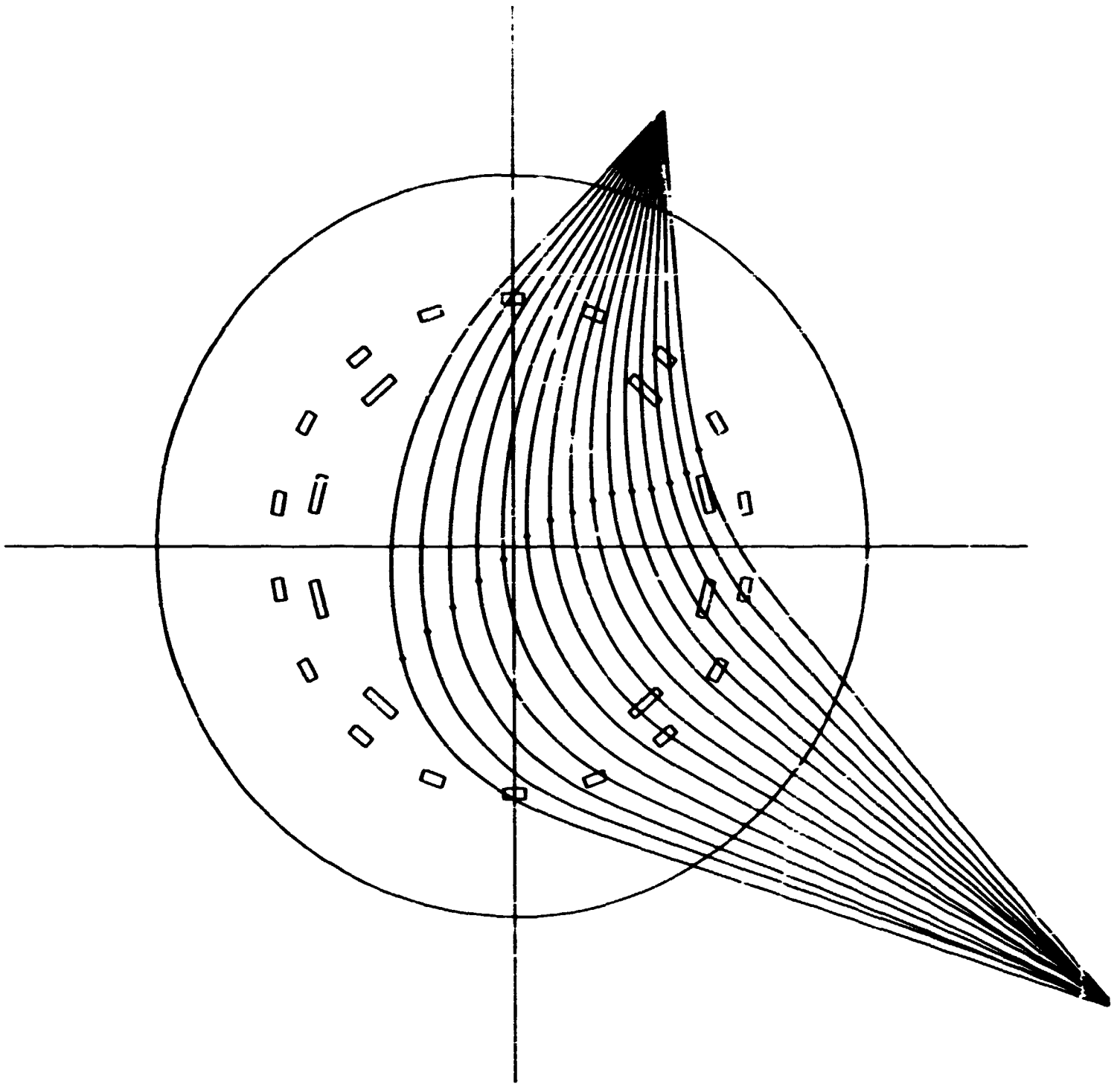

Fig. 6. Optimized Geometry for ORMAK. See Section IV for elaboration.

Figure 6 is an example of an optimized geometry. Other ion energy and geometry combinations yield similar results, but Fig. 6 displays the current design choice. The beam transmission can be further improved by slight movements of three outer coils. The coils on the y-axis will be moved toward the left half of the device, and the coil at -30° (measured from the x-axis) will be moved counterclockwise.

With fixed geometry, measurements off the plasma center can be made by changing the ion energy. Figure 7 illustrates this effect for a decreased beam energy. Increasing the beam energy moves the detector line in the opposite direction.

For EBT, two major differences from ORMAK (aside from differing magnetic fields) affect the trajectory calculations. The ions of the EBT beam probe are potassium instead of thallium, and there are no coils to intercept the beam. Two deficiencies exist in the present calculations. (1) The calculation is two dimensional. This approximation is exact in the mid-plane between two EBT coils where the ion beam will be injected. However, unlike ORMAK, the magnetic field varies strongly as a function of z, and the effect of slight displacements out of the mid-plane should be studied with three dimensional calculations. (2) The effect of the high-beta annulus is not presently accurately known and is phenomenologically approximated in the present calculations. The vacuum EBT magnetic field in the mid-plane is modified by a form factor given by

$$F(\vec{r}) = \left[1 - \frac{3}{4} \exp\left\{-\left(|\vec{r}_a| - |\vec{r} - \vec{r}_c|\right)^2/\Delta r\right\}\right]^{\frac{1}{2}} \qquad (4.4)$$

This is a gaussian depression of the vacuum field to 50 percent of normal due to an annulus of radius r_a, off center by r_c with a diffuseness of Δr. The form factor is based on the fact that

ORNL-DWG 72-10245

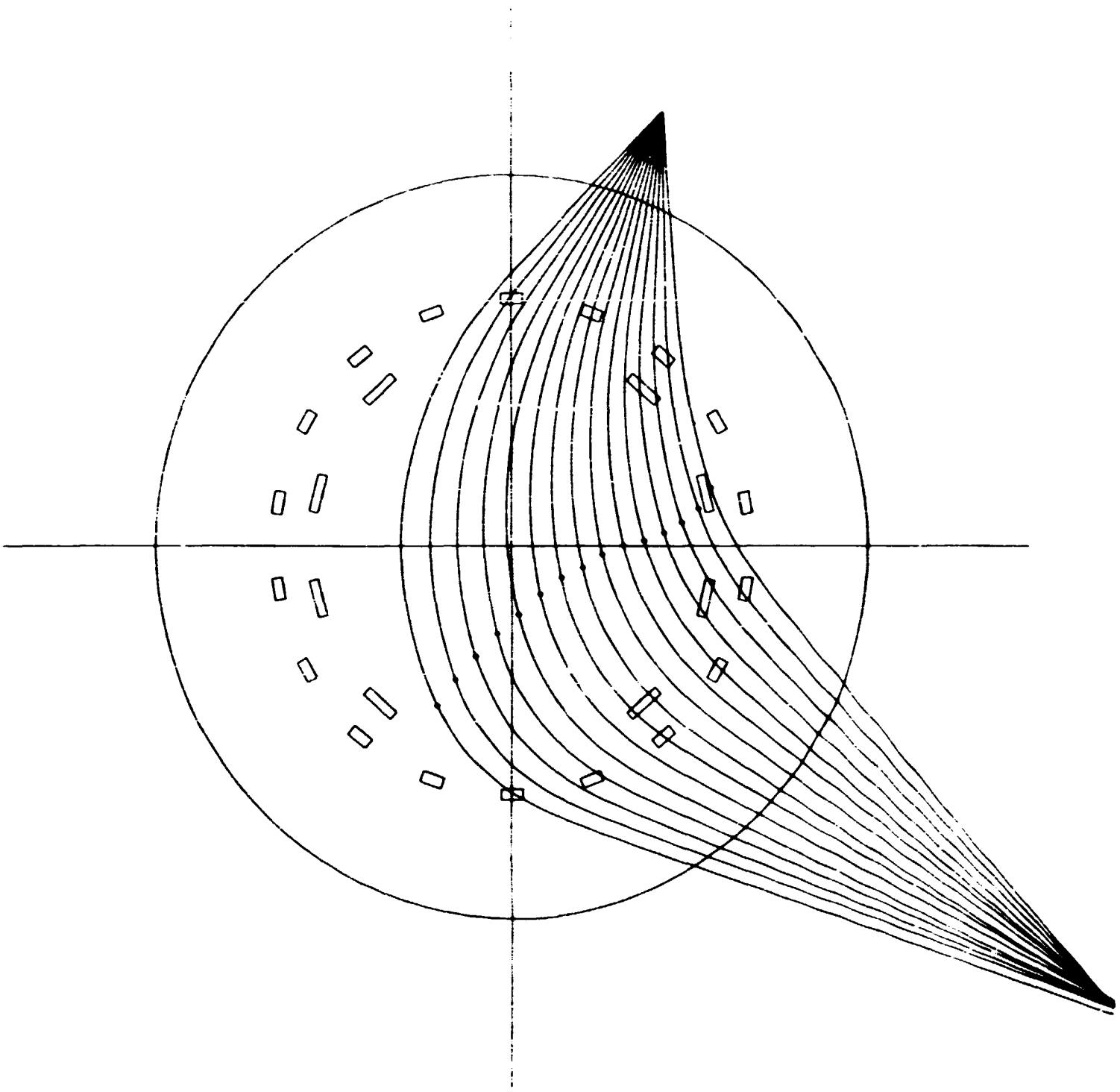

Fig. 7. Effect on the Detector Line of Varying the Ion Energy.

$$p_\perp + B^2/2 \sim \text{constant} \ , \qquad (4.5)$$

where $p_\perp$ is the perpendicular plasma pressure in the annulus, and B is the modulus of the magnetic field. The plasma pressure in the annulus falls off in an approximately gaussian manner. Scaling the proposed EBT geometry to the canted mirror results,[2] one obtains r_a = 12 cm, $\vec{r}_c$ = (-2,0,0) cm, and Δr = 23 cm[2].

Figure 8 is a trajectory calculation without the presence of the annulus, and Fig. 9 includes the above approximation to the annulus. It is clear that in the above approximation the effect of the annulus on the detector line and source-detector geometry is significant. These calculations will be continued and extended to three dimensions when the magnetic field due to the high-beta annulus is better known.

V. Results of Lens Calculations

Note that for parallel sweep plates, Eqs. 3.9 and 3.10 are independent of the ion mass. Thus, the thallium and potassium beams have identical behavior in the lens system. For a given ion energy, the lens must be designed to provide a sweep angle large enough to move the beam across the plasma volume of interest and at the same time to have a focal length long enough to isolate the lens system from the plasma. For an ion energy of 600 keV (ORMAK probe), a sweep angle of 30° and a focal length of 21 cm is produced by the lens parameters x_s = 27 cm, x_d = 60 cm, x_ℓ = 40 cm, y_ℓ = 10.2 cm, and V_c = 70 kilovolts. The transverse dispersion for a beam of one cm diameter introduced by this lens is 3.2 cm per meter. For an ion energy of 120 keV (EBT probe), a sweep angle of 37° and a focal length of 5.1 cm are produced by the lens parameters x_s = 25 cm, x_d = 60 cm,

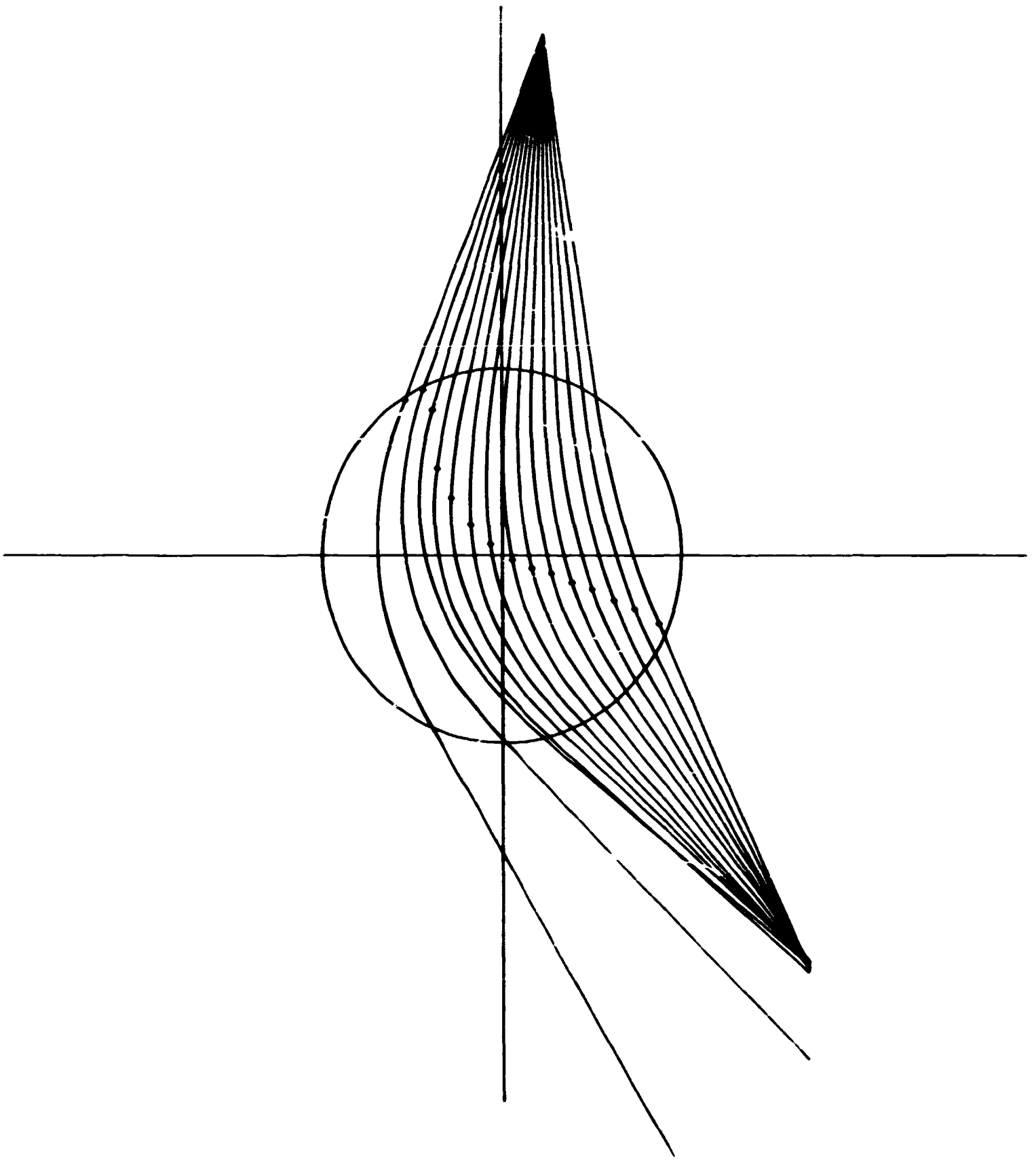

Fig. 8. Typical EBT Detector Line Without the High-Beta Annulus.

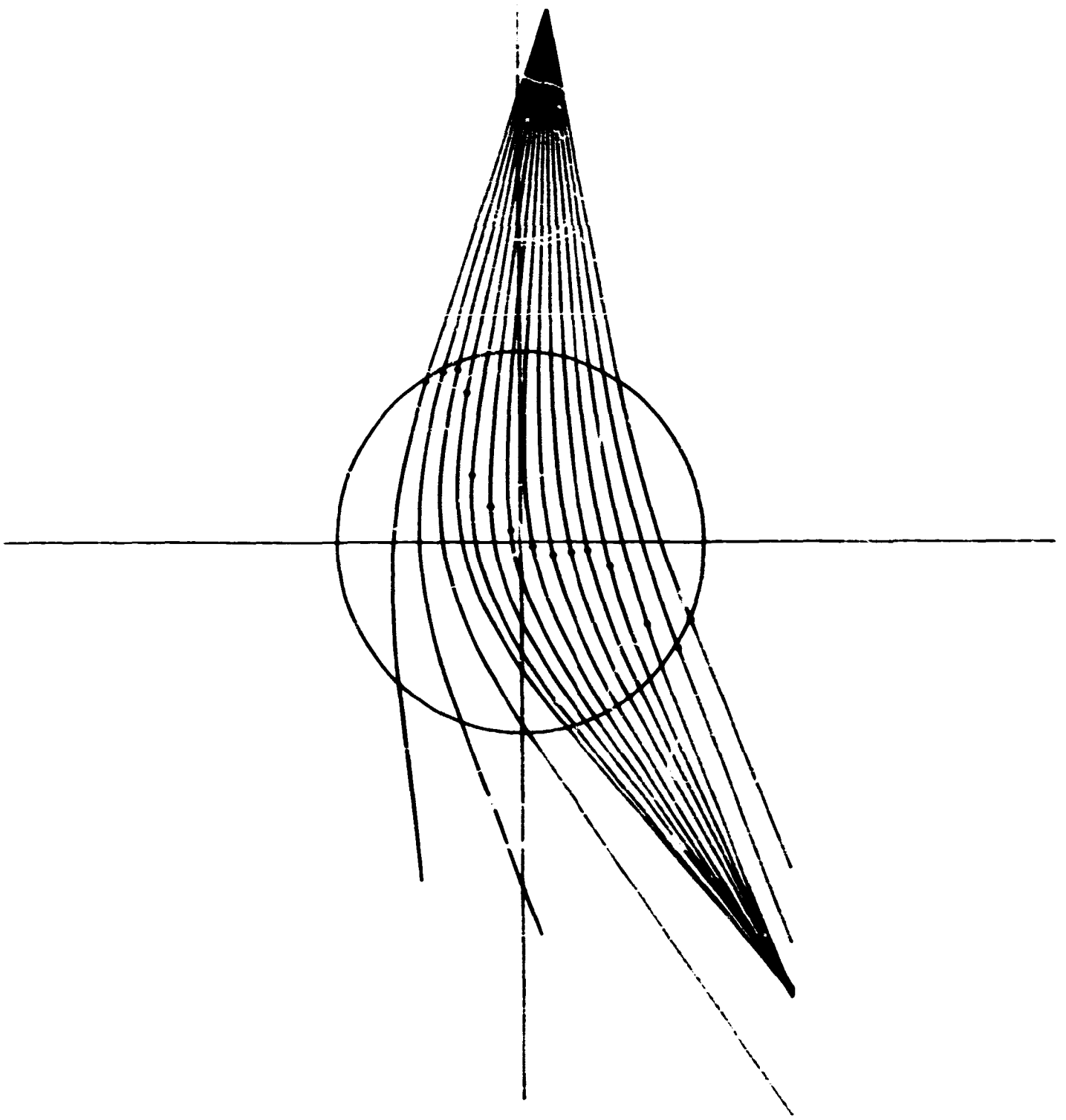

Fig. 9. Typical EBT Detector Line With the High-Beta Annulus Simulated as Described in Section IV.

x_ℓ = 30 cm, y_ℓ = 7.2 cm, and V_o = 17 kilovolts. The transverse dispersion for a beam of one cm diameter introduced by this lens is 4.8 cm per meter. The transverse dispersion is less in the ORMAK case, but the distance the beam travels before detection is longer. Thus, in both cases the transverse dispersion produced by the lens may cause significant loss of beam intensity and resolution. Therefore, it is desirable to inject the narrowest possible beam into the lens as the dispersion is roughly proportional to the diameter of the injected beam.

REFERENCES

1. G. G. Kelley et al., Conceptual Design of ORMAK Facility, ORNL-TM-2821 (1969) as amended by op. cit., Proposed Change in the ORMAK Program, ORMAK-TM-32 (1970).

2. R. A. Dandl et al., The ELMO Bumpy Torus Experiment, ORNL-TM-3694 (1971).

3. R. L. Hickok and F. C. Jobes, Ion Beam Probe for the ST Tokamak, AFOSR-TR-72-0018 (1972).

4. G. W. Westley and J. A. Watts, Editors, The Computing Technology Center Numerical Analysis Library, CTC-39, p. 114 (1970).

5. W. A. Perkins and J. C. Brown, MAFCO, A Magnetic Field Code for Handling General Current Elements in Three Dimensions, UCRL-7744 (1964).